

Monte Carlo simulation of GaN/AlN and AlN/InN mixtures

John A. Purton^{a,*}, Mikhail Yu. Lavrentiev^{b,c,1,2}, Neil L. Allan^{b,1}

^a CCLRC, Daresbury Laboratory, Warrington WA4 4AD, UK

^b School of Chemistry, University of Bristol, Cantock's Close, Bristol BS8 1TS, UK

^c Institute of Inorganic Chemistry, 630090 Novosibirsk, Russia

Received 3 May 2006; received in revised form 26 March 2007; accepted 8 April 2007

Abstract

Exchange Monte Carlo calculations in the semi-grand canonical ensemble are used to determine the mixing properties of AlN with GaN and InN in *both* the wurtzite and zinc blende structures. For $\text{In}_x\text{Al}_{1-x}\text{N}$ solid solutions the difference in structure is reflected in the properties of the phase diagrams. The calculated consolute temperature is ≈ 150 K greater for the cubic phase. The calculated phase diagrams for the two structures are significantly asymmetric with the maximum in the binodals lying markedly on the Al rich side. The $\text{Ga}_x\text{Al}_{1-x}\text{N}$ solid solution is almost ideal and no observable difference between the phase diagrams for the hexagonal and cubic structures.

© 2007 Elsevier B.V. All rights reserved.

Keywords: Monte Carlo; Phase equilibria; Nitrides

1. Introduction

The last decade has seen remarkable progress in the development of optical and electronic devices such as light-emitting diodes and laser diodes, based on the group-III nitrides AlN, GaN, InN and their alloys. Important examples are active optoelectronic devices operating in the green, blue and ultra-violet spectral region [1]. The band gaps of InN, GaN and AlN are 1.89, 3.44 and 6.28 eV, respectively [2]. Alloys of these end members have been fabricated in order to “engineer the band gap” and thus manufacture materials for novel devices.

Understanding the thermodynamic properties and atomic structure of $\text{In}_x\text{Al}_{1-x}\text{N}$ and $\text{Ga}_x\text{Al}_{1-x}\text{N}$ alloys is crucial to the systematic fabrication and development of ultraviolet and visible optoelectronic devices and multiple quantum wells (MQWs). For example, GaN/AlGaIn MQW's have been grown on (10 $\bar{1}$ 2) Al_2O_3 [3] and (100) LiAlO_2 [4]. An understanding of the phase behaviour of these materials is required for the development and fabrication of novel devices. Under ambient conditions GaN, InN, AlN and their alloys have been observed to crystallise in

the hexagonal wurtzite structure [5]. A common feature of the nitride alloy epitaxies is the strain due to the lattice mismatch and different thermal expansion coefficients. The ionic radii for Al, Ga and In in fourfold coordination are 0.39, 0.47 and 0.62, respectively [6]. For alloys the large difference in the equilibrium lattice constants and bond lengths may result in internal strain and phase separation.

Because of the potential applications of $\text{In}_x\text{Al}_{1-x}\text{N}$ and $\text{Ga}_x\text{Al}_{1-x}\text{N}$ alloys, there have been a number of theoretical studies of the mixing properties of AlN–InN and AlN–GaN and InN and these have included both the delta-lattice-parameter model [7], valence force field [8] and electronic structure calculations [9–11]. However, these studies have often relied on a limited number of atomic configurations, ignored the difference in crystal structure of the wurtzite and zincblende phases and excluded the influence of lattice vibrations on the mixing properties of $\text{In}_x\text{Al}_{1-x}\text{N}$ and $\text{Ga}_x\text{Al}_{1-x}\text{N}$ alloys. In this paper analytical potentials are derived for the Al–In–N system by fitting to experimental properties of the end member compounds. These empirical potentials are used to calculate directly the phase diagram from atomistic Monte Carlo simulations that allow us to consider the full structural relaxation around each ion present, numerous ionic configurations and thermal/vibrational effects on the crystal structure and phase diagram. We interpret and compare the mixing properties of $\text{In}_x\text{Al}_{1-x}\text{N}$ and $\text{Ga}_x\text{Al}_{1-x}\text{N}$ in both wurtzite (*h*-) and zinc blende (*c*-) forms.

* Corresponding author. Tel.: +44 1925 603785; fax: +44 1925 60388.

E-mail address: j.a.purton@dl.ac.uk (J.A. Purton).

¹ Tel.: +44 117 928 8308; fax: +44 117 925 1295.

² On leave from Institute of Inorganic Chemistry, 630090 Novosibirsk, Russia.

2. Methodology

The basis for our calculations is the well-known Monte Carlo (MC) method modified as described below. In simulations of ionic non-stoichiometric materials using “standard” MC, kinetic barriers prevent sampling the whole of the configurational space since almost always only one cation arrangement (the initial configuration), chosen at random, is sampled. We only describe briefly the Monte Carlo exchange (MCX) technique, since it has been discussed in detail in our previous papers [12,13]. In order to calculate the phase diagram *both* the atomic configuration *and* the atomic coordinates of all the atoms in the system are modified. In any one MC cycle one of four alterations to the system are made at random.

- (i) an atom is displaced by a random amount. The maximum changes in the atomic displacements are governed by a variable r_{\max} . The magnitude of this parameter is adjusted automatically during the simulation to maintain an acceptance/rejection ratio of approximately 0.5.
- (ii) a change in cell volume. The parameter v_{\max} controls the maximum allowed change in volume and is controlled in a similar manner to r_{\max} . The external pressure applied to the cell was set to 10^5 Pa.
- (iii) attempted exchange of In(Ga) and Al ions using an exchange bias technique.
- (iv) a semi-grand canonical substitution [13,14]. In this method we evaluate the potential energy change $\Delta U_{B/A}$ which would result if one species, B were to be converted into another, A. This change in energy is related to the corresponding change in chemical potential $\Delta\mu_{B/A}$ by,

$$\Delta\mu_{B/A} = -k_B T \ln \left\langle \frac{N_B}{N_A + 1} \exp \left(-\frac{\Delta U_{B/A}}{k_B T} \right) \right\rangle. \quad (1)$$

The semi-grand canonical ensemble is used in preference to the grand canonical ensemble since good statistics for $\Delta\mu_{B/A}$ can readily be achieved. The calculated values of $\Delta U_{Ga/In}$ are used to determine the excess free energy of mixing as described below. The Metropolis algorithm [15] is used to accept or reject any move, volume change or ion exchange. The Monte Carlo calculations

Table 1

Interatomic pair potential parameters for the AlN system

Atom types	A (eV)	ρ (Å)	C (eV Å ⁶)
N–N	21751.84	0.2688	20.0
Al–N	851.149	0.2985	0.00

The parameters are for the Buckingham pair potential $V_{ij} = A \exp(-r_{ij}/\rho) - Cr_{ij}^{-6}$ (see text). The parameters for GaN and InN are identical to those in [16].

were based upon simulation cells consisting of 256 ions ($4 \times 4 \times 4$ unit cells) and 216 ions ($3 \times 3 \times 3$ unit cells) for the wurtzite and zinc blende structures, respectively. The number of iterations for each simulation consisted of 2×10^6 and 5×10^7 cycles for the equilibration and production stages, respectively.

The potential model we have adopted for our simulations consists of a long-range Coulombic term and a short-range potential V_{ij} of Buckingham form:

$$V_{ij} = A \exp \left(-\frac{r_{ij}}{\rho} \right) - Cr_{ij}^{-6}. \quad (2)$$

where r_{ij} is the interionic separation between ions labelled i and j , and A , ρ and C are parameters obtained as described below. The derivation of the potential model has been discussed in detail in a previous paper and the potential parameters for GaN and InN were presented in this paper [16]. The parameters for AlN were obtained by fitting to the structure and elastic properties. The resulting interatomic potentials for AlN are listed in Table 1 and in Table 2 we compare results obtained with our new potential with experiment [17,18] and with values calculated in [19,20]. The values of our final calculated properties are in excellent agreement with experiment.

3. Results and discussion

The Monte Carlo calculations were performed on AlN–InN and AlN–GaN solid solutions adopting both the wurtzite and the

Table 2
Calculated and experimental properties of AlN

Property	AlN (this work)	AlN (experiment/ <i>ab initio</i>)	AlN [20]
wurtzite phase			
Lattice parameters (Å)			
a	3.142	3.113 ^a	3.112
c	5.043	4.981 ^a	4.970
Al–N distance (Å)	1.8998	1.8778 ^a	1.8846
	1.9564	1.8992	1.9167
Lattice enthalpy (eV/ion)	–21.37		–21.75
Elastic constants (GPa)			
C_{11}	440.6	410.5 ^b	417.4
C_{12}	151.6	148.5 ^b	178.1
C_{13}	149.0	98.9 ^b	152.0
C_{33}	393.5	388.5 ^b	432.0
C_{44}	138.6	124.6 ^b	124.6
Zinc blende phase			
Lattice parameters (Å)			
a	4.418	4.32–4.42 ^c	4.368
Al–N distance (Å)	1.913		1.8915
Lattice enthalpy (eV/ion)	–21.32		–21.71
Elastic constants (GPa)			
C_{11}	341.2	304–348 ^c	320.1
C_{12}	191.1	152–168 ^c	211.1
C_{44}	170.6	135–199 ^c	182.4

Our results are compared to experiment [17,18], *ab initio* calculations [19] and previous atomistic calculations using shell model potentials [20].

^a Edger [17].

^b Reeber and Wang [18].

^c Kim et al. [19].

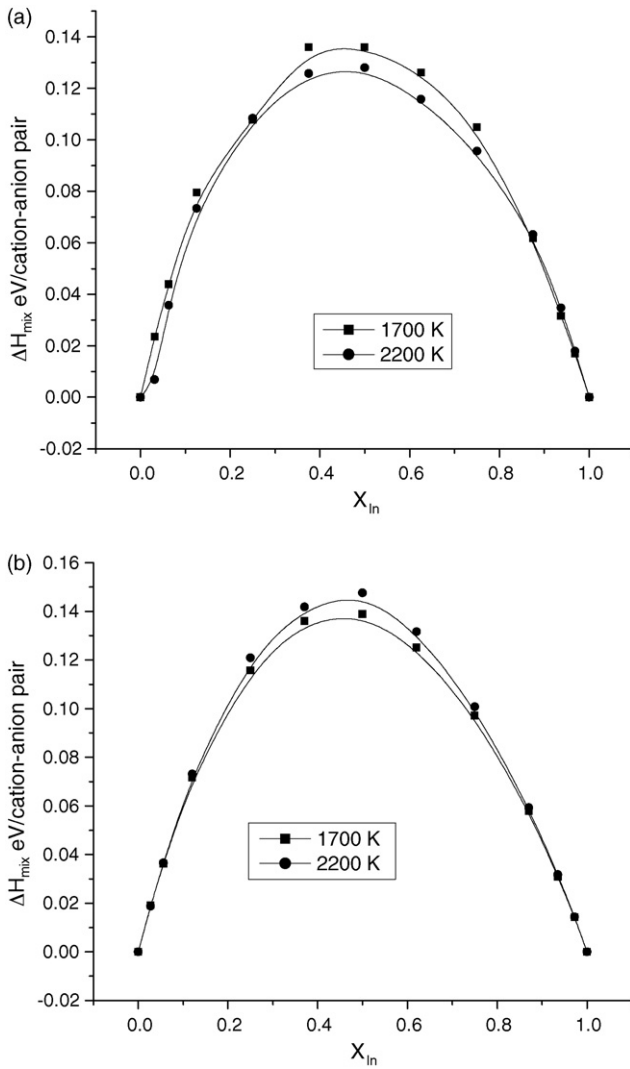


Fig. 1. Calculated values of the enthalpy of mixing, ΔH_{mix} , eV per cation–anion pair for $h\text{-In}_x\text{Al}_{1-x}\text{N}$ (a) and $c\text{-In}_x\text{Al}_{1-x}\text{N}$ (b).

zinc blende structure. During the production part of the calculations we monitored the enthalpy of the system and the chemical potential difference between Ga and In ions.

We consider first the enthalpies of mixing, ΔH_{mix} , and their variation with composition. Fig. 1a and b display the calculated values of ΔH_{mix} for the h - and c - $\text{In}_x\text{Al}_{1-x}\text{N}$ solutions over a range of temperatures. The curves have a maximum at $x \approx 0.50$. But they are not symmetric about the maximum with higher values of ΔH_{mix} on the Al rich side, *i.e.* the AlN end member accommodates In less readily than the InN lattice does Al. The phase with the smaller atom as the major species is thus less tolerant of the larger ion as a dopant than the reverse, in keeping with the general form of the cation–anion interatomic potential. It is important to stress that the method applies no constraints on the form and symmetry of the ΔH_{mix} versus composition curve. The calculated values of ΔH_{mix} at 2200 K for h - and c - $\text{In}_x\text{Ga}_{1-x}\text{N}$ at the maximum are ≈ 0.13 and 0.14 eV per cation–anion pair, respectively, *i.e.* the magnitudes of the enthalpy of mixing at 2200 K for the zinc blende and wurtzite structures are similar. Our calculated val-

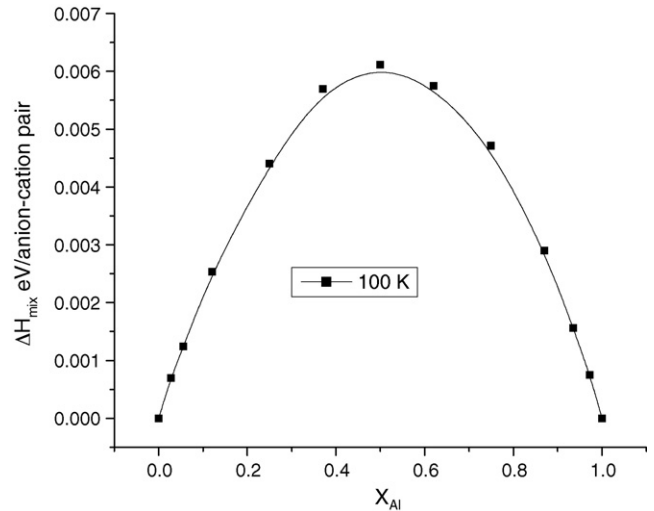


Fig. 2. Calculated values of ΔH_{mix} (eV per cation–anion pair) for $c\text{-Ga}_x\text{Al}_{1-x}\text{N}$.

ues of ΔH_{mix} are slightly greater than the value of ≈ 0.1 eV per cation–anion pair for the cubic phase in [10,11] but less than the values of 0.16 eV per cation–anion pair reported in [10] for the hexagonal phase (Ref. [10] employed a generalised quasichemical model fitted to *ab initio* pseudopotential calculations). The difference in energy for the h - and $c\text{-In}_x\text{Al}_{1-x}\text{N}$ cited in [10] is approximately 0.6 eV per cation–anion pair and is much greater than the difference observed in our calculations. The maximum values of ΔH_{mix} for h - and $c\text{-Ga}_x\text{Al}_{1-x}\text{N}$ are 0.005 and 0.006 eV per cation–anion pair, respectively and the curves are almost symmetric ($c\text{-Ga}_x\text{Al}_{1-x}\text{N}$ is displayed in Fig. 2). The calculated values in [10] are 0.01 and 0.006 eV per cation–anion pair for h - and $c\text{-Ga}_x\text{Al}_{1-x}\text{N}$, respectively. This maximum value in ΔH_{mix} for $\text{Ga}_x\text{Al}_{1-x}\text{N}$ is much lower than for the $\text{In}_x\text{Al}_{1-x}\text{N}$ and $\text{In}_x\text{Ga}_{1-x}\text{N}$ [16] alloys as would be expected from the small difference in ionic radii of Al and Ga.

The calculation of the phase diagram requires the determination of *free energy differences* rather than absolute values, which can be achieved using the semi-grand canonical ensemble described above. We show the calculated values of $\Delta\mu_{\text{Al/In}}$ in Fig. 3a and b for both the wurtzite and zinc blende structures of $\text{In}_x\text{Al}_{1-x}\text{N}$, respectively. In Fig. 4 we present only calculated values of $\Delta\mu_{\text{Al/Ga}}$ for the zinc blende phase of $\text{Ga}_x\text{Al}_{1-x}\text{N}$, since the results for the cubic and hexagonal phases are almost identical. The existence of a minimum and maximum in a $\Delta\mu_{(x)}$ curve indicates a miscibility gap at that temperature. For both phases of $\text{In}_x\text{Al}_{1-x}\text{N}$ it is clear from the shape of these curves that 1900 and 2100 K correspond to temperatures below the consolute temperature T_C , and the formation of one- and two-phase regions at different compositions. At 2100 K the stationary points have almost disappeared as this temperature is just below T_C . At 2300 and 2400 K for the h - and $c\text{-In}_x\text{Al}_{1-x}\text{N}$, respectively, the stationary points are not present, as is clear from Fig. 3, and these temperatures are above the consolute temperature. A similar conclusion can be drawn for $\text{Ga}_x\text{Al}_{1-x}\text{N}$ (Fig. 4), in which the stationary points evident at 100 K are absent at 150 K. In addition, the shape of the curves for h - and $c\text{-In}_x\text{Al}_{1-x}\text{N}$ exhibit

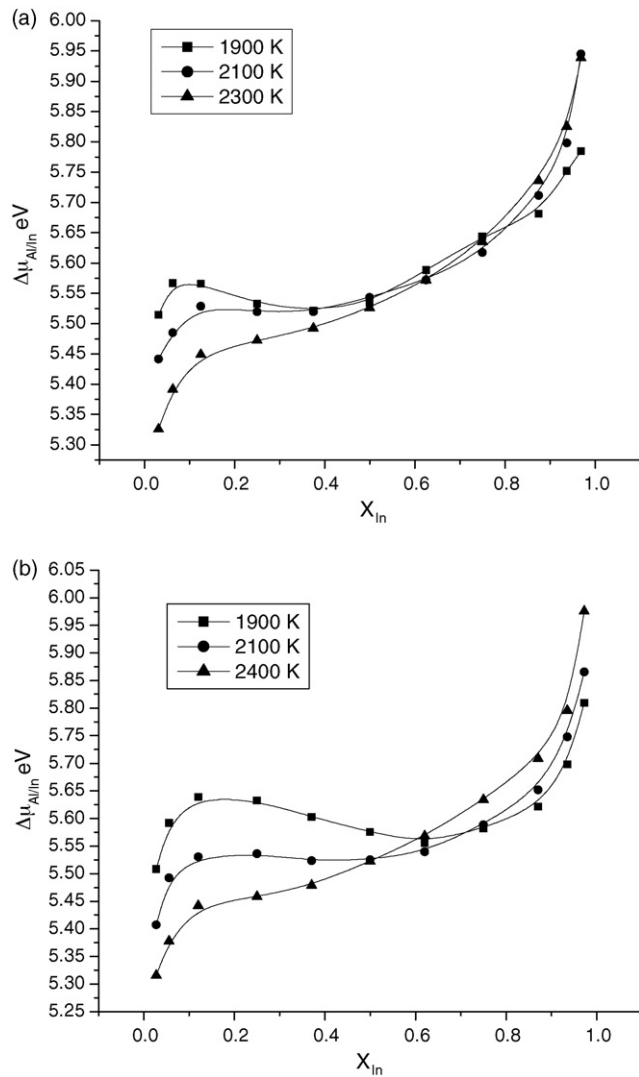


Fig. 3. Calculated variation of $\Delta\mu_{\text{Ga/In}}$ ($=\mu_{\text{In}} - \mu_{\text{Al}}$) as a function of $\text{In}_x\text{Al}_{1-x}\text{N}$ alloy composition for (a) wurtzite; and (b) zinc blende structures.

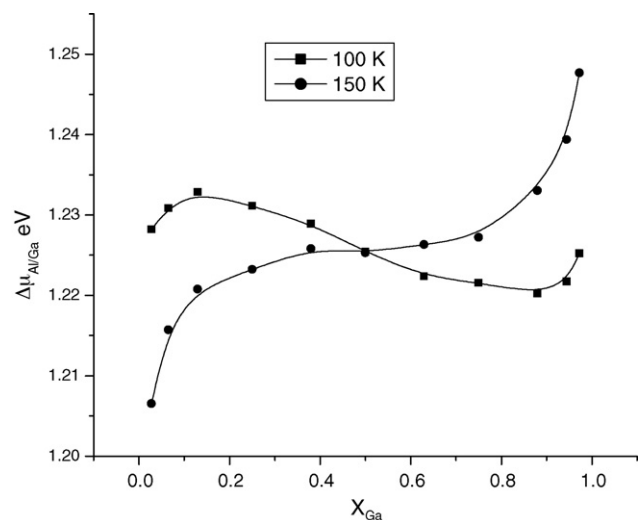


Fig. 4. Calculated variation of $\Delta\mu_{\text{Al/Ga}}$ ($=\mu_{\text{Ga}} - \mu_{\text{Al}}$) as a function of $\text{Ga}_x\text{Al}_{1-x}\text{N}$ alloy composition for the zinc blende structure.

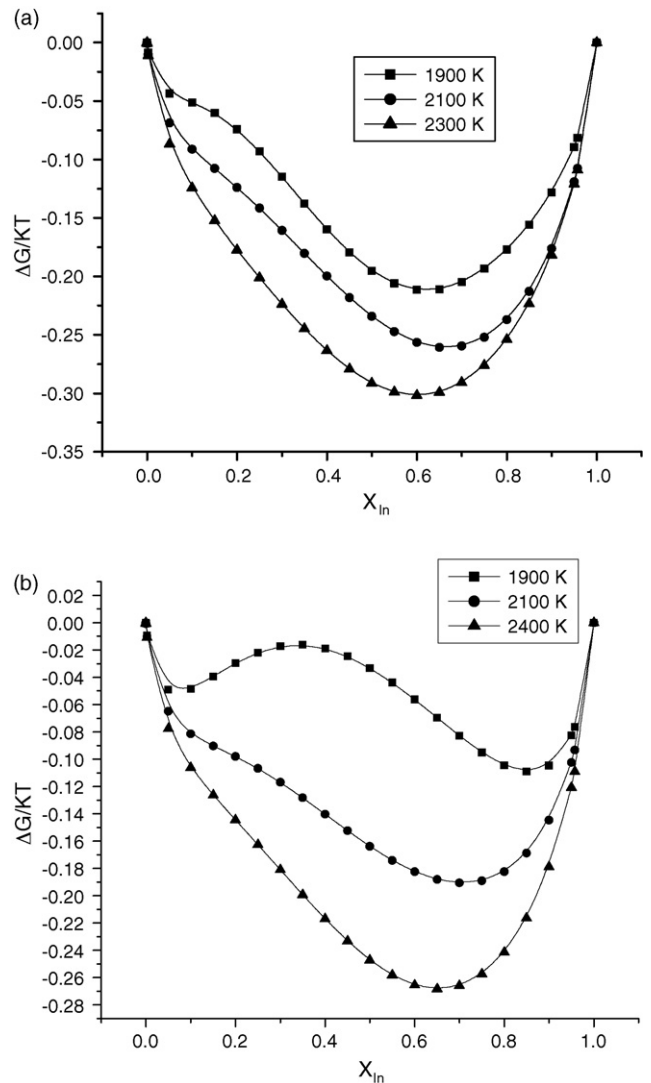


Fig. 5. Calculated variation of ΔG_{mix} for $\text{In}_x\text{Al}_{1-x}\text{N}$ with alloy composition for (a) wurtzite; and (b) zinc blende structures.

significant differences and we expect this to be reflected in the calculated phase diagram.

To calculate the phase diagram, the calculated values of $\Delta\mu(x)$ are fitted [13] to Eq. (3), as shown by the full lines in Fig. 3:

$$\frac{\Delta\mu}{k_{\text{B}}T} = \ln\left(\frac{x}{1-x}\right) + ax + bx^2 + cx^3. \quad (3)$$

By integrating Eq. (3) with respect to composition we obtain the variation in free energy with x at each temperature. In Fig. 5a and b we plot calculated values of ΔG_{mix} versus x over a range of temperatures for h - and c - $\text{In}_x\text{Al}_{1-x}\text{N}$, respectively. Fig. 5 confirms that for h - and c - $\text{In}_x\text{Ga}_{1-x}\text{N}$ at 1900 and 2100 K, one- and two-phase regions are formed at different compositions, and hence that this temperature lies below the consolute temperature. At 2300 and 2400 K, the dependence of $\Delta G_{\text{mix}}(x)$ at all compositions is consistent with complete miscibility for both h - and c - $\text{In}_x\text{Al}_{1-x}\text{N}$, respectively. Given curves as in Fig. 5, a straightforward common tangent construction at each temperature yield

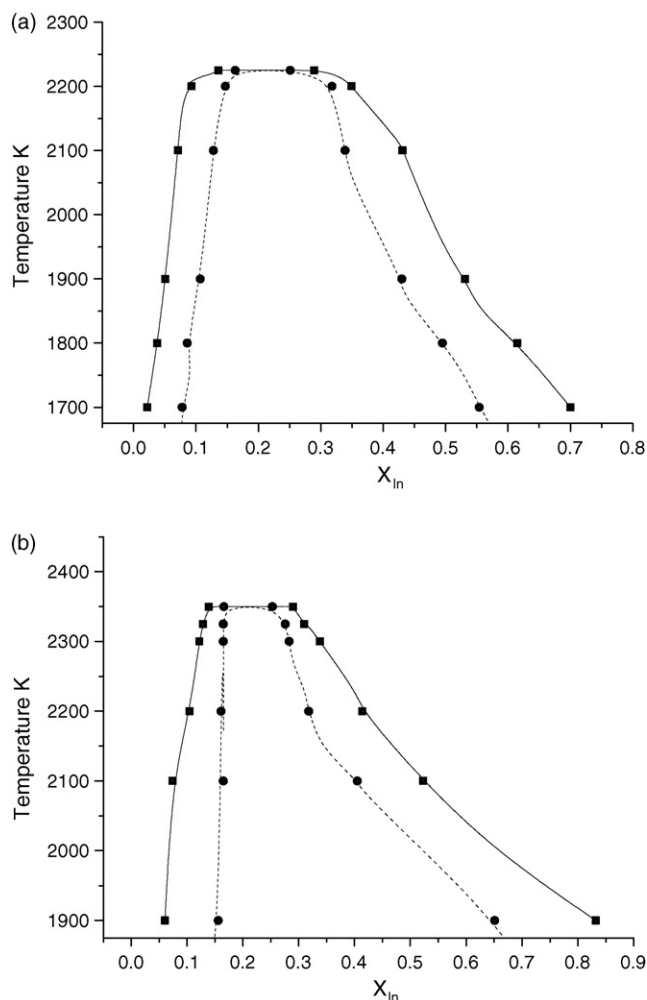


Fig. 6. Calculated phase diagram for (a) *h*- and (b) *c*- $\text{In}_x\text{Al}_{1-x}\text{N}$. Solid squares mark the binodal and solid circles the spinodal.

the phase diagrams in Fig. 6a and b. Thus, by performing calculations at several temperatures, the consolute temperatures were determined to be 2225 ± 13 and 2375 ± 13 K for the hexagonal and cubic phases, respectively. The consolute temperature calculated using alternative methodologies range from 1474 to 3400 K [14–17]. As in the calculations reported in [10], we find that the binodal curves are highly asymmetric, and slanted towards the Al end member such that the apex is at $x \approx 0.2$, *i.e.* the Al ion is more soluble in InN than In in AlN. Although the consolute temperature of both phases is similar, there are important differences between the phase diagrams. The phase diagram for *h*- $\text{In}_x\text{Al}_{1-x}\text{N}$ is more asymmetric than that for the cubic form and Al is more soluble in *h*- $\text{In}_x\text{Al}_{1-x}\text{N}$ than in *c*- $\text{In}_x\text{Al}_{1-x}\text{N}$. Calculations on $\text{In}_x\text{Ga}_{1-x}\text{N}$ have also also demonstrated an asymmetry but to a lesser extent [16] As expected the $\text{In}_x\text{Ga}_{1-x}\text{N}$ phase diagram is almost symmetric and demonstrates that mixing of GaN and AlN is almost ideal (Fig. 7). The spinodal curves are also plotted in the phase diagrams in Figs. 6 and 7 and define the region where a single phase is kinetically as well as thermodynamically unstable with respect to the formation of two separate phases.

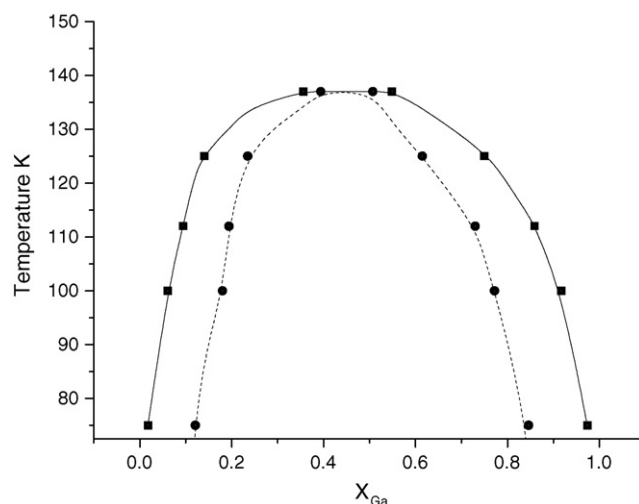


Fig. 7. Calculated phase diagram for *c*- $\text{Ga}_x\text{Al}_{1-x}\text{N}$. Solid squares mark the binodal and solid circles the spinodal.

4. Conclusions

We have derived a set of interatomic potentials for the system AlN and employed these potentials with those of [16] to study the Al–In–N and Al–Ga–N systems. These potentials have been demonstrated to reproduce accurately the properties of the end member compounds. The MC calculations, based on these interatomic potentials, have been undertaken to calculate the phase diagrams of $\text{In}_x\text{Al}_{1-x}\text{N}$ and $\text{In}_x\text{Ga}_{1-x}\text{N}$. The MC calculations take into account local relaxations and the vibrational effects of the ions and can be applied to different crystal structures of the same compound. With this in mind, we have determined the mixing properties of AlN and InN/GaN in *both* the wurtzite and zinc blende structures. The difference in the enthalpies of mixing is reflected in the structure of the phase diagrams. The calculated consolute temperature for the $\text{In}_x\text{Al}_{1-x}\text{N}$ solid solution is approximately 2225 and 2375 K for both the hexagonal and cubic phases, respectively. The phase diagram has a pronounced asymmetry, which is a result of asymmetry in both the excess enthalpy and excess entropy of mixing. For $\text{In}_x\text{Ga}_{1-x}\text{N}$, mixing is almost ideal and for the two structures an identical phase diagram is observed (within uncertainties in the calculation). We hope our paper prompts further experimental studies of this interesting system and we hope to develop our computational work to include surfaces and thin films.

References

- [1] S. Nakamura, G. Fasol, *The Blue Laser Diode*, Springer, Berlin, 1997.
- [2] Y. Wu, B.P. Keller, S. Keller, D. Kapolnek, P. Kosodoy, S.P. Denbaars, J.K. Mishra, *Appl. Phys. Lett.* 69 (1996) 1438.
- [3] R. Langer, J. Simon, V. Ortiz, N.T. Pelekanos, A. Barski, R. Andre, M. Godlewski, *Appl. Phys. Lett.* 74 (1999) 3827.
- [4] N.M. Ng, *Appl. Phys. Lett.* 80 (2002) 4369.
- [5] K. Osamura, S. Naka, Y. Murakami, *Solid State Commun.* 11 (1972) 617.
- [6] R.D. Shannon, C.T. Prewitt, *Acta Cryst. B* 25 (1969) 925.
- [7] T. Matsuoka, *Appl. Phys. Lett.* 71 (1997) 106.
- [8] T. Takayama, M. Yuri, K. Itoh, T. Baba, J.S. Harris Jr., *J. Cryst. Growth* 222 (2001) 29.

- [9] M. van Schilfgaarde, A. Sher, A.-B. Chen, *J. Cryst. Growth* 178 (1997) 8.
- [10] L.K. Teles, J. Furthmüller, L.M.R. Scolfaro, J.R. Leite, F. Bechstedt, *Phys. Rev. B* 62 (2000) 2475.
- [11] M. Ferhat, F. Bechstedt, *Phys. Rev. B* 65 (2002) 075213.
- [12] J.A. Purton, G.D. Barrera, M.B. Taylor, N.L. Allan, J.D. Blundy, *J. Phys. Chem. B* 102 (1998) 5202.
- [13] M.Yu. Lavrentiev, N.L. Allan, G.D. Barrera, J.A. Purton, *J. Phys. Chem. B* 105 (2001) 3594.
- [14] D. Frenkel, B. Smit, *Understanding Molecular Simulation*, second ed., Academic Press, San Diego and London, 2002.
- [15] N.L. Metropolis, A.W. Rosenbluth, M.N. Rosenbluth, A. Teller, E. Teller, *J. Chem. Phys.* 21 (1953) 1087.
- [16] J.A. Purton, M.Yu. Lavrentiev, N.L. Allan, *J. Mater. Chem.* 15 (2005) 785.
- [17] J.H. Edger (Ed.), *Properties of Group-III Nitrides EMIS data review series*, INSPEC, London, 1994, p. 11.
- [18] R.R. Reeber, K. Wang, *MRS Internet J. Nitride Semicond. Res.* 6 (2001), Article 3.
- [19] K. Kim, W.R.L. Lambrecht, B. Segall, *Phys. Rev. B* 53 (1996) 16310.
- [20] J.A. Chisholm, D.W. Lewis, P.D. Bristowe, *J. Phys.: Condens. Matter* 11 (1999) L235.